Carbon 185 (2021) 376–383

Contents lists available at ScienceDirect

Carbon

journal homepage: www.elsevier.com/locate/carbon

Research Paper

Spectroscopic insight of low energy electron emission from diamond surfaces

Gary Wan [a, b, *], Mattia Cattelan [c, d], Alex Croot [e], Hugo Dominguez-Andrade [e], Shannon S. Nicley [f, g, h], Ken Haenen [f], Neil A. Fox [b, c, e]

[a] Bristol Centre for Functional Nanomaterials, University of Bristol, Tyndall Avenue, Bristol BS8 1TL, UK
[b] Bristol Centre for Nano Science and Quantum Information, University of Bristol, Tyndall Avenue, Bristol BS8 1FD, UK
[c] School of Chemistry, University of Bristol, Cantocks Close, Bristol BS8 1TS, UK
[d] Sincrotrone Trieste S.C.p.A., Area Science Park, I-34012 Basovizza, Trieste, Italy
[e] School of Physics, HH Wills Physics Laboratory, University of Bristol, Tyndall Avenue, Bristol BS8 1TL, UK
[f] Institute for Materials Research (IMO), Hasselt University, Belgium & IMOMEC, IMEC vzw, Diepenbeek, Belgium
[g] Michigan State University, Department of Electrical and Computer Engineering, 428S. Shaw Ln., Rm. 2120, East Lansing, MI, 48824, USA
[h] Fraunhofer USA Inc., Center Midwest, Coatings and Diamond Technologies Division, 1449 Engineering Research Ct., East Lansing, MI, 48824, USA

ARTICLE INFO

Article history:
Received 11 June 2021
Received in revised form
12 September 2021
Accepted 17 September 2021
Available online 22 September 2021

Keywords:
Diamond
Thermionic emission
Spectroscopy
Surface states
Photoemission

ABSTRACT

Low work function materials are desirable in many applications such as electron emission and photocatalysis. We have studied low energy electron emission from low work function hydrogen terminated diamond surfaces via electron spectroscopy to gain insight into the mechanisms involved during electron excitation and emission. Electron emission was found to be dominated by electrons within the band gap energy region, allowed due to the negative electron affinity diamond surface, while sub-bandgap illumination was able to significantly increase emission current. Substantial upward surface band bending greater than 2 eV was observed for the diamond samples, which affect electron accumulation at the surfaces. Intra-bandgap states are shown to strongly influence electron emission behavior, which can have great implications for various energy conversion devices.

1. Introduction

Thermionic emission involves the removal of electrons from within a material after absorbing energies greater than the work function (WF), sharing similarities to that of secondary electron emission or photoemission, but simply using thermal energy to overcome the surface potential barrier[1]. This simplicity in generating free electrons allows it to form the basis of a variety of devices such as electron guns, X-ray sources, magnetrons and energy converters[2] [–] [6]. Improvements to the thermionic emission will increase energy efficiency and device performance, while minimizing fatigue over time with reduced operating temperatures.

During the thermionic emission process, the electron thermal energy distribution allows a portion of electrons to occupy surface electronic states above the vacuum level, which can then escape through the surface. Thermionic emission current is thus dependent on the density of states (DOS), temperature and WF of the material, and can be approximated for bulk metals using the Richardson-Dushman equation[1].

$$J = AT^2 e^{-\frac{\Phi}{k_B T}}, \quad (1)$$

where J is the current density, A is a material dependent constant, T is the temperature and Φ is the WF. With an exponential dependence on the WF, the emission current can be significantly increased using lower WF materials. Although the equation does not take into account the true DOS of the material, by assuming it is free-electron-like, it has generally provided good approximation for a material's WF and thermionic emission profiles. However, it may be less likely to predict thermionic emission behavior from semiconductors due to the existence of a band gap.

Diamond is a wide-bandgap semiconductor that can exhibit low

* Corresponding author. Bristol Centre for Functional Nanomaterials, University of Bristol, Tyndall Avenue, Bristol BS8 1TL, UK.
E-mail address: gary.wan@bristol.ac.uk (G. Wan).

https://doi.org/10.1016/j.carbon.2021.09.045

WF when nitrogen or phosphorus doped and terminated with hydrogen to produce a negative electron affinity (NEA) surface, such that the vacuum level lies below the surface conduction band minimum (CBM)[7]. When considered with other properties such as vacuum stability and extremely high thermal conductivity, diamond is a strong candidate for thermionic emitter material. However, nitrogen and phosphorus doped diamond (NDD and PDD) have a high activation energy unlike boron doped diamond (BDD) acceptor levels[8,9]. This leads to reduced electrical conductivity until relatively high temperatures, as well as an increased barrier for electron emission.

While the temperature-dependent current density from Equation (1) provides quantitative information on the thermionic emission capabilities, it lacks insight on the origins of electrons as well as their energy distribution. Here we have used electron spectroscopy to study the mechanisms involved in thermionic emission from diamond surfaces, which allows for detailed investigation of electronic states and their occupancy. By observing electron emission as a function of electron kinetic energy rather than the total emission current, effects on the energetic emission intensities arising from the WF, band gap, band bending and electron affinity can be visualized.

2. Methods and materials

Phosphorus, nitrogen and boron doped polycrystalline diamond were grown on 10 mm × 10 mm nano-diamond seeded silicon substrates in a microwave-enhanced plasma chemical vapor deposition (CVD) reactor. The PDD was prepared at Hasselt University by microwave plasma enhanced chemical vapor deposition (MWPECVD) in a 2.45 GHz ASTeX PDS17 Microwave plasma-assisted CVD reactor with a water cooled molybdenum substrate holder[10]. The total flow rate was 500 SCCM with 0.5% CH_4 in H_2, and 1% PH_3 in CH_4. A constant forward microwave power of 2500 W and pressure of 70 Torr was used for a growth duration of 3 h.

The NDD and BDD were grown at the University of Bristol, using an ASTeX-type 2.45 GHz MWPECVD reactor. The total gas flow rate was 312 SCCM with 4% CH_4 in H_2, where 2.5% N_2 and 100 ppm B_2H_6 was used respectively in CH_4 for the NDD and BDD. A forward microwave power of 1500 W and pressure of 150 Torr was used, for a growth duration of 30 min. All samples were then hydrogen terminated using the MWPECVD reactor using 300 SCCM of H_2 at 800 °C and 500 °C for 2 min each. The hydrogen termination was confirmed using contact angle measurements[11,12], showing angles of about 100° in Fig. S1.

The samples were then transferred into the ultra-high vacuum (UHV) chambers at the Bristol NanoESCA Facility, where they were annealed at 300 °C for 1 h before analysis and remained under UHV for the remainder of the experiment. The thermal annealing under vacuum cleans the diamond surface and removes any surface conductivity resulting from the negative electron affinity and surface adsorbates[13].

Electron spectroscopy was performed using a hemispherical analyzer with a pass energy of 6 eV, for an analyzer energy resolution of about 300 meV. A bias of 20 V was placed between the sample and analyzer during analysis to overcome the analyzer work function. Heating of the sample during measurements was done via a resistive heating filament behind the sample, where the current-dependent sample temperature was pre-calibrated. A monochromated Al-Kα X-ray source and white LED lights were also used as excitation light sources for some measurements.

3. Results and discussion

Scanning electron microscopy (SEM) of the two samples are shown in Fig. 1, showing a micro-crystalline diamond structure. The images show no specific crystallographic orientation, meaning that emissions observed are an average of all the present surface orientations. While WF variations commonly exist between different surface orientations[14], their contributions are insignificant for the studies done here. The surface morphology difference between the PDD and NDD are insignificant and thus any emission differences are attributed to the different dopants. It should also be noted that for other electron emission mechanisms such as field emission, the diamond surface morphology and grain boundaries can play a crucial role[15,16], thus the Raman spectra for the two samples are shown in Fig. S2 for reference. Fig. S3a also shows an electron emission microscope of a diamond surface during thermionic emission, indicating that thermionic emission was generally uniform on the microscopic scale, in agreement with other works in the literature[17].

As shown from beta-radiation enhanced emissions, the energy distribution of excited electrons also play an important role towards the emission current[18]. Even at thermal equilibrium, determining the electron energy distribution can also be extremely beneficial towards understanding electron emission from low WF semiconducting surfaces. The spectroscopy of the thermionic emission is therefore performed on the low WF polycrystalline PDD and NDD from Fig. 1.

Electron emission and thermal peak broadening were studied using sample temperatures between 300 and 700 °C. Emission at lower temperatures were not tested due to the reduced electrical conductivity of the PDD and NDD, and the insignificant amount of thermionic emission current below 300 °C; while thermal desorption of hydrogen would likely begin at temperatures around 700 °C[19] [–] [21], which would lead to changes in the electron affinity, WF and surface band bending[22] [–] [25].

X-ray photoelectron spectroscopy (XPS) was performed on the samples at elevated temperatures, where the C 1*s* core level is shown in Fig. 2. The C 1*s* binding energies for the hydrogen terminated PDD and NDD are approximately 286.5 eV, about 2 eV higher than typically observed for BDD. This can be explained by the slight n-type doping induced on the PDD and NDD, where the Fermi level (E_F) is closer to the CBM in the bulk, in contrast to the p-type doping in BDD with the E_F near the VBM. The binding energy is the energy difference between E_F and a core-level, thus a higher E_F position will shift the core-level spectra to higher binding energies. The wide band gap in diamond allows for large changes in E_F position and thus binding energies with chemical doping.

With the higher E_F of PDD and NDD, the shift to higher binding energies for their C 1*s* peaks relative to a BDD is to be expected[26], though the magnitude of the shift is significantly less than suggested from simple comparison between their bulk donor level positions in diamond. With the E_F at 0.37 eV above the VBM for BDD [27], 1.7 and 0.56 eV below the CBM for NDD and PDD respectively [8,28], a C 1*s* binding energy shift of 3.4 and 4.6 eV is expected. This indicates a downward band bending for the p-type and significant upward band bending for n-type diamond surfaces.

Surface band bending is difficult to precisely determine using XPS due to contributions from different depth within the material [29], and the theoretical calculations needed for such comparisons. The elevated temperatures used also affect the carrier concentration and thus band bending amount, while also broadening spectral peaks. However, the relative band bending between a hydrogen and bare termination can be observed. The unterminated samples were prepared by thermal desorption of the hydrogen terminated surfaces at 900 °C within the UHV chambers after completion of other measurements. The dotted lines in Fig. 2 show the C 1*s* emission spectra of bare diamond surfaces, indicating an increase in upward band bending by approximately 0.5 eV. This is consistent

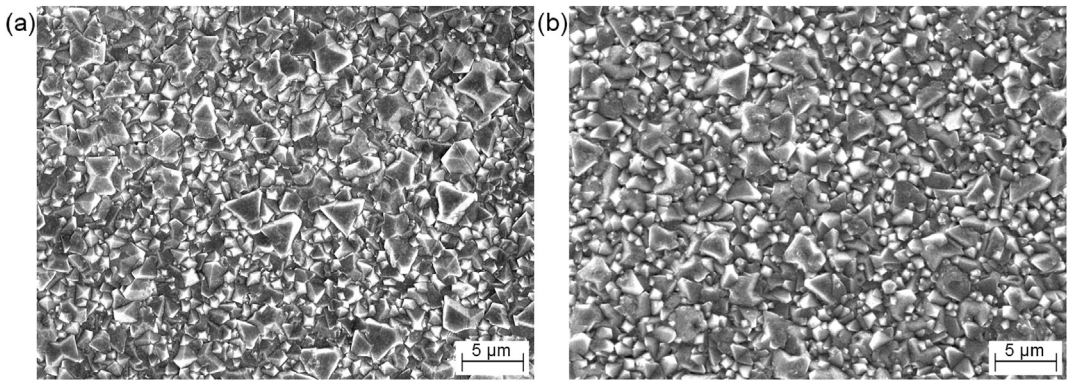

Fig. 1. SEM images of the (a) PDD and (b) NDD.

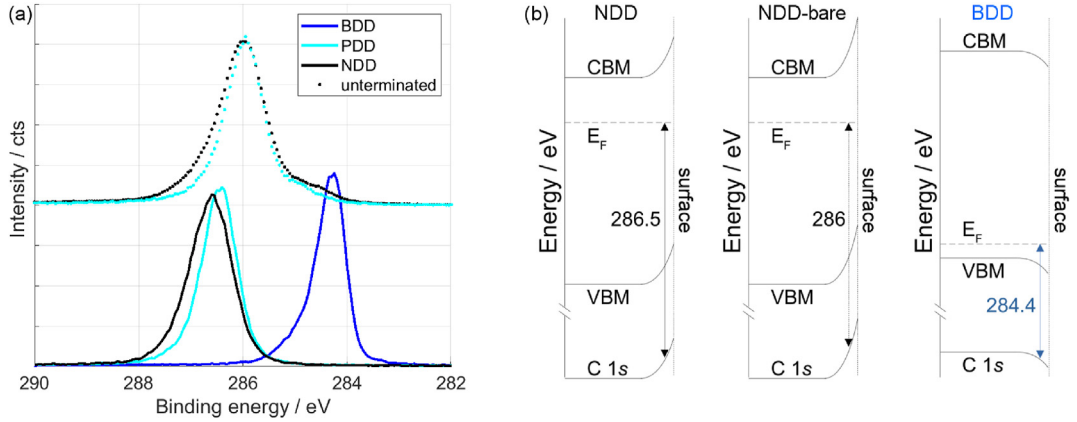

Fig. 2. (a) XPS of the C 1*s* peak for the polycrystalline hydrogen terminated PDD (blue), PDD (cyan) and NDD (black). The unterminated samples are in dotted lines and vertically shifted. (b) Band diagrams of the NDD (left), unterminated NDD (right) and BDD (right). (A colour version of this figure can be viewed online.)

with previous studies where hydrogen termination was shown to induce a downward surface band bending on diamond[22].

The low kinetic energy region of the electron emission can also be used to determine the band alignments, though with a significantly greater surface sensitivity than the energy region used for the XPS in Fig. 2 [30]. A slight charging of up to 0.2 eV was observed for the NDD due to insufficient conductivity at 300 °C, where an increase in emission current lead to a greater voltage drop across the sample. Contributions to the electron emission in this region can include thermionic emission, photoemission from low-energy light sources and secondary electron emission[31] [–] [35].

We begin with the emission spectra from the PDD and NDD surface at 300 °C in Fig. 3, where a single peak between 2 and 2.5 eV above E_F is observed. Without any charging, the low-energy cutoff indicates the position of the vacuum level, and hence the WF of the surface. Emission with the additional excitation from white LED lights are also shown in dotted lines, where an increase in emission intensity was observed, showing that even low energy photons can excite electrons from doped diamond into the vacuum, or at least promote carrier transport to the surface. This is significant for photon enhanced thermionic emission and diamond photocatalytic devices[4] [–] [6,36], and helps explain observation of enhanced photocatalysis when using sub-bandgap radiation[37]. To ensure the intensity increase in emission is not from localized spots during LED illumination, microscopy of the thermionic emission was done using an energy-filtered photoemission electron microscope setup in Fig. S3, where the emission increase appears uniform over the sample surface. The increased emission from LED lights are also observed at higher temperatures, as shown in Fig. S4 for the samples at 400 °C, where the featured emission peaks can potentially be due to defect-induced states[5,6].

To further investigate the enhanced electron emission from sub-bandgap illumination on diamond, two laser sources were also used on the PDD. A red laser diode showed no noticeable difference in the thermionic emission behavior, while a 5 mW 532 nm (2.33 eV) green laser showed enhancements, indicating a lower limit for the photon energy required. The emission spectra using the green laser on the PDD at 300 and 400 °C are shown in Fig. 4. Other than increases in the overall emission intensity, the emission line shape also shows slight differences, which can be further investigated using tunable photon sources. The interactions between the initial and final states in photo-assisted thermionic emission can also be predicted with computational theory[38,39].

Sub-bandgap excitation and emission using low energy light sources can have significant implications for a wide range of devices and applications. For example in diamond-based thermionic energy converters where significant advances towards obtaining ultra-low WF materials have been achieved[40], the phosphorus or nitrogen doped diamond can have a further enhancement of performance under optical illumination. This would be convenient for solar-based converters, and may allow for lower operating temperatures as well. Other possibilities include taking advantage of the photoexcitation process for semiconducting purposes, where doped diamond substrates can be used as a photo-conductive semiconducting switch[41]. Understanding and optimizing the electron excitation process may lead to breakthroughs in diamond

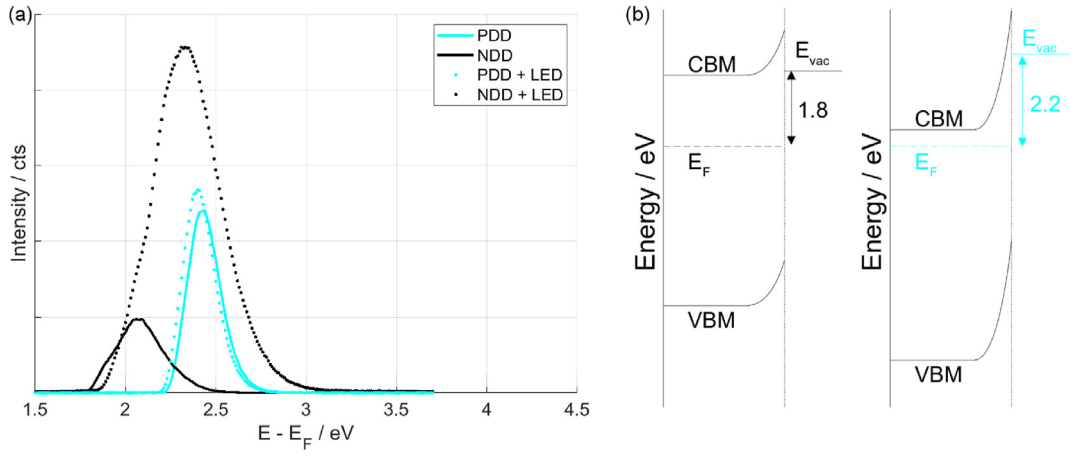

Fig. 3. (a) Low energy electron emission from PDD (cyan) and NDD (black) at 300 °C. Spectra with LED excitation is shown with dotted lines. (b) Band diagrams for the NDD (left) and PDD (right). (A colour version of this figure can be viewed online.)

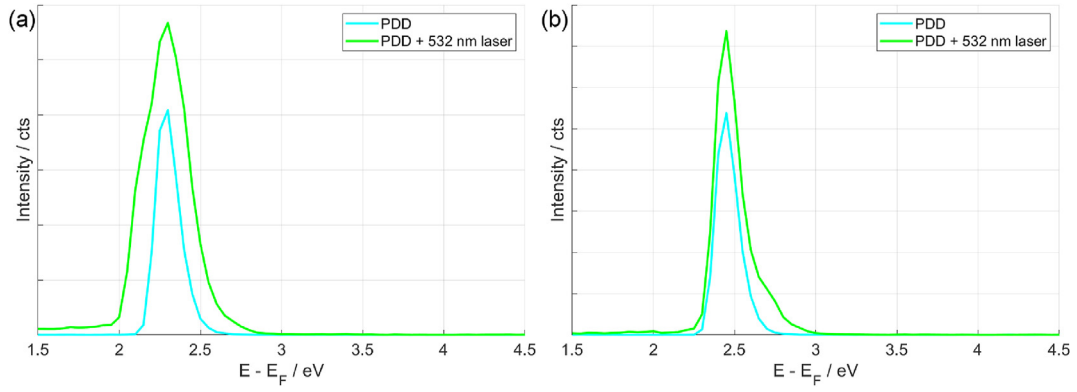

Fig. 4. The thermionic emission spectra from the hydrogen terminated PDD surface with and without 532 nm laser illumination, at (a) 300 °C and (b) 400 °C. (A colour version of this figure can be viewed online.)

semiconducting devices, where the n-type conductivity has often been a limiting factor.

The emission intensity for the NDD increased significantly more than on the PDD after the additional LED excitation, which can be due to different doping concentrations of nitrogen and phosphorus in the diamond. As phosphorus doping efficiency into the diamond structure is significantly lower than nitrogen[10,28], a greater density of states at the donor level in NDD can allow for greater absorption efficiency of the LED light. However, with the shallower phosphorus donor level in the PDD, a greater bulk conductivity can be achieved at 300 °C, leading to a reduced shift of the peak to lower energies from charging. The broader NDD peak is also likely due to differential charging across the sample surface. This shows the importance of both doping concentration and the dopant thermal activation energies.

Emission spectra from a hydrogen terminated BDD sample is shown in Fig. 5 for comparison, where no emission was observed without using X-ray illumination. The WF is noticeably higher at approximately 3.5 eV, which would explain its lack of thermionic emission and photoemission from LED lights in contrast to the PDD and NDD. To provide the extra energy needed for emission, X-rays were used to generate pure secondary electrons without direct photoemission from occupied states. Under X-ray illumination, emission was observed where electrons thermalize into unoccupied states and are emitted as secondary electrons. A peak with a broad shoulder towards the low-energy cutoff is observed on the BDD, which was previously studied and attributed to the CBM emission at the peak, and intra-bandgap emission at the shoulder [7,35]. Similar to the XPS results in Fig. 2, while a significant WF difference of over 1.2 eV is observed between the BDD and the n-type samples, it is significantly less than the difference between their bulk E_F positions. The downward band bending on the BDD decreases its WF while also allowing for electron accumulation in the CBM at the surface, giving rise to the large peak around 5 eV [29]. A small amount of electron emission was still observed for several minutes after the X-ray illumination as shown in orange in Fig. 5, likely also owing to the downward band bending as well as the indirect diamond band gap contributing to the longer lifetime of excited electrons. The n-type PDD and NDD however exhibit upward band bending which draw surface electrons at the CBM into the bulk, in turn causing secondary electrons to accumulate less near the CBM. This highlights the dominating effect of band bending on low-energy surface emission.

The two n-type samples were then heated up to 400 °C for further analysis, where a significant increase in emission intensity was observed (Fig. 6), as predicted by the Richardson equation in Equation (1). Other notable differences include the shape of the low-energy peak, where a double peak can now be observed, with a separation of approximately 0.1 eV. A double peak is generally expected for hydrogen terminated diamond due to its NEA providing emission peaks at the CBM and vacuum level[7], though the separation is typically in the region of 1 eV[25]. Given the energy

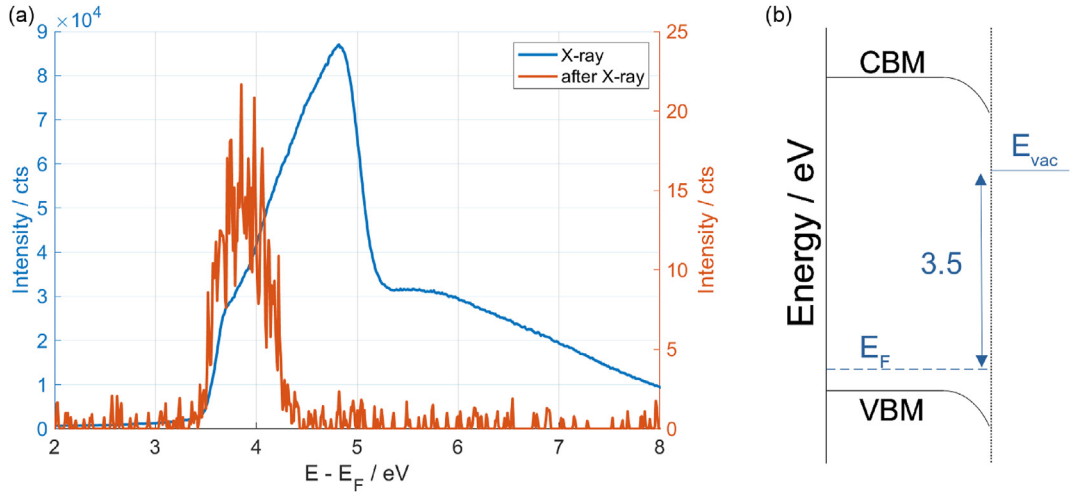

Fig. 5. (a) Low energy electron emission from BDD at 300 °C using X-ray excitation (blue), and immediately after switching off the X-ray source (orange). (b) Band diagram of the BDD showing a downward band bending. (A colour version of this figure can be viewed online.)

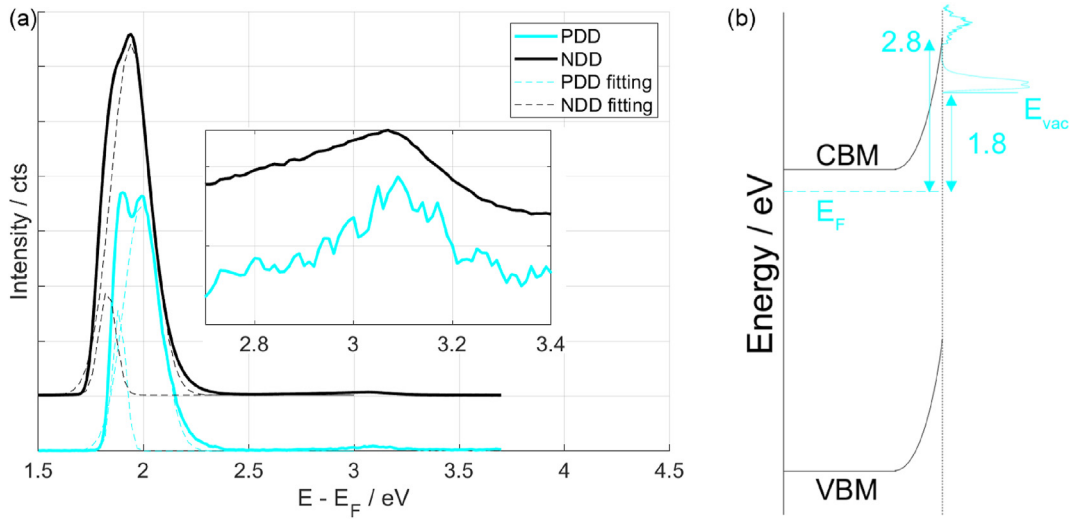

Fig. 6. (a) Thermionic emission spectra of the (cyan) PDD and (black) NDD at 400 °C, the NDD spectrum is vertically shifted and normalized for visibility. A two-component Gaussian fitting is used for the peaks at around 2 eV, and shown in dashed lines. The inset shows a zoomed in region near 3 eV. (b) Band diagram of the PDD with the emission peaks superimposed. (A colour version of this figure can be viewed online.)

position of the observed peaks, they likely originate from within the band gap, indicating spectral features at the surface near the vacuum level. Angle-resolved measurements of secondary electrons on hydrogen terminated BDD (100) and (111) surfaces at room temperature however show no observable surface states in this region[35]. The difference in emission behavior is therefore either a temperature or band bending effect.

Potential explanations include existence of surface states outside the free-electron parabola horizon, which are disallowed emissions due to the lack of momentum matching with vacuum states[35,42], and therefore not observed with secondary electron emission. However, while under sufficient thermal excitation, electrons in these states may be inelastically scattered and emitted into the vacuum. The effect was likely not observed in Fig. 3 due to the significantly lower population of the state at 300 °C. Another possibility is that the surface dipole induced by a hydrogen termination may have additional effects on the electric field near the surface[21], producing localized states where electrons can be excited from, similar to those seen with image potentials[43].

The inset in Fig. 6 shows a magnified view of the spectra at around 3 eV where the intensity increases again after tailing off from the first peak near 2 eV. The intensity of this peak is substantially lower than the initial peak, which can be expected due to the thermal occupancy of electronic states in accordance with the Boltzmann distribution. The reduction in intensity between 2.2 and 2.8 eV therefore indicates a lower density-of-states than at 3 eV. Separation between the two observed emission peaks is roughly 1 eV, which is consistent with the expected NEA of hydrogen terminated diamond surfaces. These observations further confirm that the low-energy emission cutoff is at the vacuum level and lies within the band gap, whereas the emission near 3 eV is at the surface CBM position.

Thermal energy at 400 °C is shown to be sufficient to populate and emit a small proportion of electrons from the surface CBM, which lies at about 2.8 eV above E_F for both the PDD and NDD. A noticeable degree of Fermi-level pinning is therefore shown to exist for diamond, though the pinning amount is not entirely constant. As seen with the BDD in Fig. 5, the CBM position to be

approximately 4.8 eV above E_F, showing that the surface Fermi level position can be altered with sufficient doping. The difference in measured band bending between the BDD and n-type diamond determined in this low-energy region can differ from XPS in Fig. 2, due to the greater bulk contributions when using XPS[29,30]. Comparing to the bulk Fermi level positions of the PDD and NDD samples, a significant amount of upward band bending of 2.2 and 1.1 eV respectively is obtained. This resulted in the emission being almost completely dominated by electron emission within the band gap, particularly at lower temperatures. For thermionic emission devices, surface states at the band gap and a large NEA value are therefore critical to performance.

The PDD and NDD were then annealed to 900 °C within the same UHV chamber to desorb hydrogen from the surface, while minimizing surface graphitization. This leaves a predominantly unterminated bare diamond surface, which has been reported to exhibit a slight positive electron affinity (EA) and affect the surface band bending[44]. The increased EA and upward surface band bending would therefore result in an increased WF and reduction in electron emission, which was characterized by further spectroscopy near the work function threshold.

The emission spectra for unterminated PDD and NDD at different temperatures are shown in Fig. 7 with X-ray excitation, which was necessary for emission below 600 °C. The low energy threshold for emission up to 600 °C is approximately 4.5 eV for the unterminated samples, indicating a significantly increased CBM position from the 2.8 eV of the hydrogen terminated surface. The exact CBM position for the unterminated samples may be lower than the emission threshold due to the slight PEA of unterminated diamond surfaces (0.38 eV)[44].

Above 600 °C, the emission spectra for both samples show a lower energy emission peak beginning at 3 eV that is unaffected by the X-ray excitation. This shows that secondary electrons at the CBM are extremely inefficient at populating the surface states within the band gap, whereas thermally excited electrons can be directly emitted from those states. For the NDD, the peak position relative to the CBM (~ 1 eV below) fits well with previous spectra of the hydrogen terminated surfaces, indicating that the emissions were likely from residual hydrogen terminated sites after the thermal desorption by annealing. The small amount of hydrogen did not appear to induce any changes in the local surface band bending, seen from its position relative to the CBM peak, indicating insignificant changes to the surface state occupancy. Meanwhile, significant broadening of peaks were observed for the unterminated PDD, likely a result of inhomogeneous and strong upward band bending across the surface from its low dopant density and lack of hydrogen termination.

The PDD sample was later exposed to atmosphere when partially hydrogen terminated before being tested again, significantly reducing its emission intensity. Contact angle measurements of a hydrogen desorbed sample after air exposure shows contact angles of about 65°, indicating a significantly decreased hydrophobicity after removal of hydrogen[11,12], compared with the contact angle of hydrogen terminated diamond in Fig. S1. Fig. 8 shows the emission spectra from 300 to 500 °C with and without LED excitation, where the two distinct peaks observed earlier in Fig. 6 are observed and have varying height dependence on the thermal and LED excitation. The two peaks at around 3 eV correspond to the double peaks observed on the hydrogen terminated diamond, while the higher energy region from the conduction band was also observed when using X-ray excitation (not shown). The conduction band peaks while not explicitly shown and magnified in Fig. 8a, can be barely observed at precisely 1 eV higher energy than the taller LED peak in red. The constant energy spacing between those two peaks even as the WF and bend bending changes with temperature strongly suggest the LED illumination peak is from a band feature.

Focusing back onto the two main features seen in Fig. 8a, it is clear that thermionic emission only contributes to the lower energy peak at lower temperatures, while the LED lights promote emission from the second peak without any noticeable effect on the first peak. This is a particularly interesting observation as the LED is a low-energy non-monochromatic source, which is successfully exciting a narrow distinct peak without affecting emission at a lower energy. The possibility of sub-bandgap radiation absorption from intermediate states has also been discussed for laser irradiated diamond substrates[5,6]. The two peaks from each LED illumination spectra have been decomposed into two Gaussian components, and a small shift in relative energy position is observed between different temperatures, unlike mentioned above for the second peak and the conduction band. This is likely due to small WF changes on the sample surface with temperature, as the

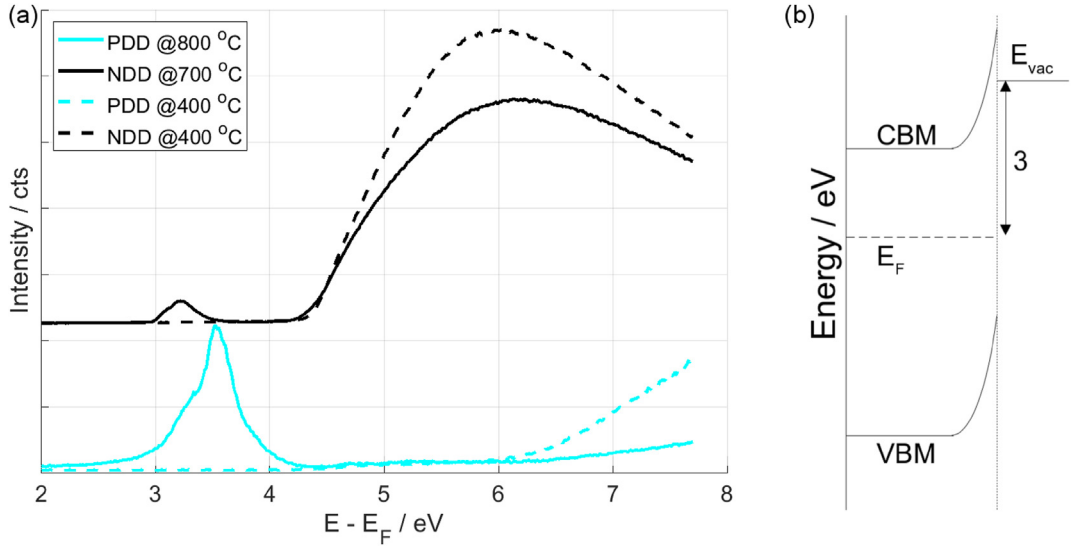

Fig. 7. (a) Emission spectra of the bare PDD (cyan) and NDD (black) samples under X-ray illumination. The solid lines are at 800 °C for the PDD and 700 °C for the NDD, while the dotted lines are at 400 °C. The NDD spectra are shifted vertically for visibility. (b) The NDD band diagram. (A colour version of this figure can be viewed online.)

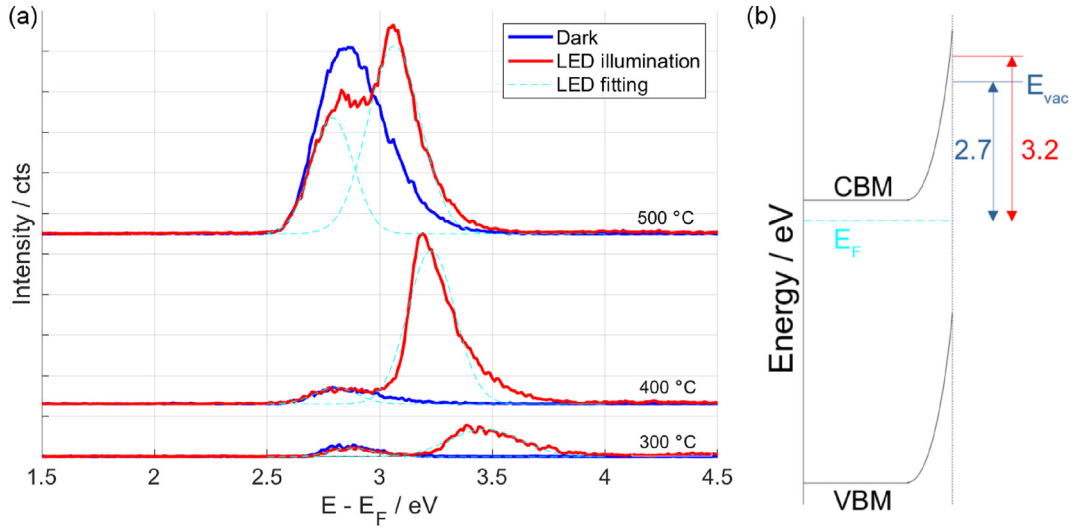

Fig. 8. (a) Emission spectra of the PDD after air exposure, from 300 to 500 °C, with (red) and without (blue) LED excitation. The dashed lines are peak fittings for the LED illuminated spectra, showing the two components. (b) Band diagram of the PDD with the position of the two emission peaks indicated. (A colour version of this figure can be viewed online.)

lowest energy peak position is determined by the WF cutoff of electron emission. Therefore, the lower energy peak of the two is unlikely to originate from a band feature.

The energy range of a typical LED extends to approximately 2.7 eV, meaning that any direct electronic excitation into the state at 3.2 eV above E_F in Fig. 8 must have an initial state above E_F. This indicates that there are sufficiently occupied states within the band gap and above the Fermi level at 300 °C, while the states at 3.2 eV are initially unoccupied without LED excitation. This is in agreement with the proposal of intra-bandgap surface states mentioned above and potentially of electron photoexcitation from image-potential like states[43], but into a final state rather than directly into the vacuum due to the narrow peak width. The lack of decay into the lower energy first peak also suggests a long lifetime of the surface state at 3.2 eV, or no direct decay pathway. LED excitation of the second peak also increases with temperature, which is consistent with the theory of initial states being above E_F, as they increase in occupation with temperature. The thermally excited first peak is likely to be from surface emissions at the vacuum level rather than a surface state[35,45], which could explain its lack of response towards photoexcitation. For applications in air or under solution, the additional states induced by surface adsorbates may further enhance photon capture.

4. Conclusion

Spectroscopic measurements of thermionically emitted electrons provide insight into mid-bandgap energy levels in diamond, showing interesting properties of hydrogen terminated diamond. Detailed investigation shows a double peak exists near the vacuum level, where the higher energy component may indicate existence of a surface state. At lower temperatures, electron emission from below the CBM essentially contributed the entire thermionic emission current. Fermi-level pinning was found to be significant for both the nitrogen and phosphorus doped diamond, leading to upward band bending of up to 2.2 eV, therefore higher doping concentration is likely more important than lower activation energy dopants for electron emission devices. While perhaps most interestingly, low energy excitation from LED light was found to significantly increase emission current at low temperatures, which can prove very useful for devices in energy conversion or photocatalysis, and encourages further investigation to exploit a potential extremely efficient photoemitter.

CRediT authorship contribution statement

Gary Wan: Conceptualization, Methodology, Validation, Formal analysis, Investigation, Writing – original draft, Writing – review & editing, Visualization. **Mattia Cattelan:** Methodology, Validation, Formal analysis, Investigation, Writing – original draft, Visualization. **Alex Croot:** Conceptualization, Validation, Formal analysis, Investigation, Writing – original draft. **Hugo Dominguez-Andrade:** Conceptualization, Validation, Resources, Writing – original draft. **Shannon S. Nicley:** Conceptualization, Validation, Resources, Writing – original draft. **Ken Haenen:** Validation, Resources, Writing – original draft, Funding acquisition. **Neil A. Fox:** Resources, Writing – original draft, Supervision, Project administration, Funding acquisition.

Declaration of competing interest

The authors declare that they have no known competing financial interests or personal relationships that could have appeared to influence the work reported in this paper.

Acknowledgments

The authors acknowledge the Bristol NanoESCA Facility for experimental work (EPSRC Strategic Equipment Grant EP/K035746/1 and EP/M000605/1). This work was also financially supported by the Methusalem NANO network and the Research Foundation Flanders - (FWO) via project G0D4920N. G. Wan acknowledges the Ph.D. studentship from Renewtec Technologies funded through BCFN.

Appendix A. Supplementary data

Supplementary data to this article can be found online at https://doi.org/10.1016/j.carbon.2021.09.045.

References

[1] S. Dushman, Thermionic Emiss. Rev. Mod. Phys. 2 (1930) 381.

[2] L. Piazza, D. Masiel, T. LaGrange, B. Reed, B. Barwick, F. Carbone, Design and implementation of a fs-resolved transmission electron microscope based on thermionic gun technology, Chem. Phys. 423 (2013) 79.
[3] R.L. Jepsen, M.W. Muller, Enhanced emission from magnetron cathodes, J. Appl. Phys. 22 (1951) 1196.
[4] J.W. Schwede, I. Bargatin, D.C. Riley, B.E. Hardin, S.J. Rosenthal, Y. Sun, F. Schmitt, P. Pianetta, R.T. Howe, Z.-X. Shen, N.A. Melosh, Photon-enhanced thermionic emission for solar concentrator systems, Nat. Mater. 9 (2010) 762.
[5] P. Calvani, A. Bellucci, M. Girolami, S. Orlando, V. Valentini, R. Polini, D.M. Trucchi, Black diamond for solar energy conversion, Carbon N. Y. 105 (2016) 401.
[6] M. Girolami, L. Criante, F. Di Fonzo, S. Lo Turco, A. Mezzetti, A. Notargiacomo, M. Pea, A. Bellucci, P. Calvani, V. Valentini, D.M. Trucchi, Graphite distributed electrodes for diamond-based photon-enhanced thermionic emission solar cells, Carbon N. Y. 111 (2017) 48.
[7] L. Diederich, O. Küttel, P. Aebi, L. Schlapbach, Electron emission and NEA from differently terminated, doped and oriented diamond surfaces, Diam. Relat. Mater. 8 (1999) 743.
[8] V. Baranauskas, B.B. Li, A. Peterlevitz, M.C. Tosin, S.F. Durrant, Nitrogen-doped diamond films, J. Appl. Phys. 85 (1999) 7455.
[9] S. Koizumi, M. Kamo, Y. Sato, H. Ozaki, T. Inuzuka, Growth and characterization of phosphorous doped 111 homoepitaxial diamond thin films, Appl. Phys. Lett. 71 (1997) 1065.
[10] W. Janssen, S. Turner, G. Sakr, F. Jomard, J. Barjon, G. Degutis, Y.-G. Lu, J. D'Haen, A. Hardy, M.V. Bael, J. Verbeeck, G.V. Tendeloo, K. Haenen, Substitutional phosphorus incorporation in nanocrystalline CVD diamond thin films, Phys. Status Solidi Rapid Res. Lett. 8 (2014) 705.
[11] L. Mosińska, P. Popielarski, K. Fabisiak, A. Dychalska, Effects of hydrogen termination of CVD diamond layers, Opt. Mater. 101 (2020), 109676.
[12] O. Dunseath, E.J.W. Smith, T. Al-Jeda, J.A. Smith, S. King, P.W. May, A.H. Nobbs, G. Hazell, C.C. Welch, B. Su, Studies of Black Diamond as an antibacterial surface for Gram Negative bacteria: the interplay between chemical and mechanical bactericidal activity, Sci. Rep. 9 (2019) 8815.
[13] F. Maier, M. Riedel, B. Mantel, J. Ristein, L. Ley, Origin of surface conductivity in diamond, Phys. Rev. Lett. 85 (2000) 3472.
[14] O. Renault, R. Brochier, A. Roule, P.-H. Haumesser, B. Krömker, D. Funnemann, Work-function imaging of oriented copper grains by photoemission, Surf. Interface Anal. 38 (2006) 375.
[15] J. Robertson, Mechanisms of electron field emission from diamond, diamond-like carbon, and nanostructured carbon, J. Vac. Sci. Technol. B Microelectr. Nanom. Struct. 17 (1999) 659.
[16] R.L. Harniman, O.J. Fox, W. Janssen, S. Drijkoningen, K. Haenen, P.W. May, Direct observation of electron emission from grain boundaries in CVD diamond by PeakForce-controlled tunnelling atomic force microscopy, Carbon N. Y. 94 (2015) 386.
[17] F.A.M. Köck, J.M. Garguilo, R.J. Nemanich, Imaging electron emission from diamond film surfaces: N-doped diamond vs. nanostructured diamond, Diam. Relat. Mater. 10 (2001) 1714.
[18] A. Croot, G. Wan, A. Rowan, H.D. Andrade, J.A. Smith, N.A. Fox, Beta radiation enhanced thermionic emission from diamond thin films, Front. Mech. Eng. 3 (2017) 1.
[19] C. Su, Thermal desorption of hydrogen from the diamond C(100) surface, Surf. Sci. 406 (1998) 149.
[20] M.T. Schulberg, C.A. Fox, G.D. Kubiak, R.H. Stulen, Hydrogen desorption from chemical vapor deposited diamond films, J. Appl. Phys. 77 (1995) 3484.
[21] H. Dominguez-Andrade, J. Anaya, A. Croot, M. Cattelan, D.J. Twitchen, M. Kuball, N.A. Fox, Correlating thermionic emission with specific surface reconstructions in a < 100 > hydrogenated single-crystal diamond, ACS Appl. Mater. Interfaces 12 (2020), 26534.
[22] G. Wan, M. Cattelan, N.A. Fox, Electronic structure tunability of diamonds by surface functionalization, J. Phys. Chem. C 123 (2019) 4168.
[23] F. Maier, R. Graupner, M. Hollering, L. Hammer, J. Ristein, L. Ley, Hydrogenated and bare diamond (110) surface: a combined LEED-, XPS-, and ARPES study, Surf. Sci. 443 (1999) 177.
[24] S. Kumaragurubaran, T. Yamada, S. Shikata, Vacuum-annealing induced band bending in phosphorus-doped (111) diamond, Diam. Relat. Mater. 17 (2008) 1969.
[25] J. Cui, R. Graupner, J. Ristein, L. Ley, Electron affinity and band bending of single crystal diamond (111) surface, Diam. Relat. Mater. 8 (1999) 748.
[26] L. Diederich, O. Küttel, P. Ruffieux, T. Pillo, P. Aebi, L. Schlapbach, Photoelectron emission from nitrogen- and boron-doped diamond (100) surfaces, Surf. Sci. 417 (1998) 41, natexlaba.
[27] R.F. Mamin, T. Inushima, Conductivity in boron-doped diamond, Phys. Rev. B Condens. Matter 63 (2001) 1.
[28] K. Haenen, A. Lazea, J. Barjon, J. D'Haen, N. Habka, T. Teraji, S. Koizumi, V. Mortet, P-doped diamond grown on (110)-textured microcrystalline diamond: growth, characterization and devices, J. Phys. Condens. Matter 21 (2009), 364204.
[29] L. Diederich, O. Küttel, P. Aebi, L. Schlapbach, Electron affinity and work function of differently oriented and doped diamond surfaces determined by photoelectron spectroscopy, Surf. Sci. 418 (1998) 219, natexlabb.
[30] M.P. Seah, W.A. Dench, Quantitative electron spectroscopy of surfaces: a standard data base for electron inelastic mean free paths in solids, Surf. Interface Anal. 1 (1979) 2.
[31] V.S. Robinson, Y. Show, G.M. Swain, R.G. Reifenberger, T.S. Fisher, Thermionic emission from surface-terminated nanocrystalline diamond, Diam. Relat. Mater. 15 (2006) 1601.
[32] K. Uppireddi, T.L. Westover, T.S. Fisher, B.R. Weiner, G. Morell, Thermionic emission energy distribution from nanocrystalline diamond films for direct thermal-electrical energy conversion applications, J. Appl. Phys. 106 (2009), 043716.
[33] T. Sun, F.A.M. Koeck, C. Zhu, R.J. Nemanich, Combined visible light photoemission and low temperature thermionic emission from nitrogen doped diamond films, Appl. Phys. Lett. 99 (2011), 202101.
[34] J. Yater, A. Shih, R. Abrams, Electron transport and emission properties of C(100), Phys. Rev. B Condens. Matter 56 (1997) R4410.
[35] G. Wan, A. Croot, N.A. Fox, M. Cattelan, Empty-state band mapping using momentum-resolved secondary electron emission, Adv. Funct. Mater. 31 (2021), 2007319.
[36] D. Zhu, L. Zhang, R.E. Ruther, R.J. Hamers, Photo-illuminated diamond as a solid-state source of solvated electrons in water for nitrogen reduction, Nat. Mater. 12 (2013) 836.
[37] S. Li, J.A. Bandy, R.J. Hamers, Enhanced photocatalytic activity of diamond thin films using embedded Ag nanoparticles, ACS Appl. Mater. Interfaces 10 (2018) 5395.
[38] M. Upadhyay Kahaly, S. Misra, S.K. Mishra, Photo-assisted electron emission from illuminated monolayer graphene, J. Appl. Phys. 121 (2017), 205110.
[39] S. Madas, S.K. Mishra, S. Kahaly, M.U. Kahaly, Superior photo-thermionic electron emission from illuminated phosphorene surface, Sci. Rep. 9 (2019), 10307.
[40] F.A.M. Koeck, R.J. Nemanich, Advances in thermionic energy conversion through single-crystal n-type diamond, Front. Mech. Eng. 3 (2017) 1.
[41] D.L. Hall, L.F. Voss, P. Grivickas, M. Bora, A.M. Conway, P. Scajev, V. Grivickas, Photoconductive switch with high sub-bandgap responsivity in nitrogen-doped diamond, IEEE Electron. Device Lett. 41 (2020) 1.
[42] A. Damascelli, Probing the electronic structure of complex systems by ARPES, Phys. Scripta T109 (2004) 61.
[43] S. Tan, A. Argondizzo, C. Wang, X. Cui, H. Petek, Ultrafast multiphoton thermionic photoemission from graphite, Phys. Rev. X 7 (2017), 011004.
[44] J.B. Cui, J. Ristein, L. Ley, Electron affinity of the bare and hydrogen covered single crystal diamond (111) surface, Phys. Rev. Lett. 81 (1998) 429.
[45] R.F. Willis, N.E. Christensen, Secondary-electron-emission spectroscopy of tungsten: angular dependence and phenomenology, Phys. Rev. B 18 (1978) 5140.